

CT 100485

# MATERIALS RESEARCH in AECL




FALL 1972

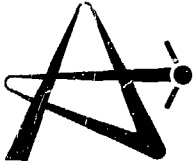


## AECL-4353

The reviews in this document are intended to give the reader a resume of materials research at Atomic Energy of Canada Limited. Those who wish to obtain more detail of the work reported in this document can request copies of the literature cited and the published progress reports of the appropriate Divisions. Application should be made to: The Scientific Document Distribution Office, Atomic Energy of Canada Limited, Chalk River, Ontario, Canada.



Micrograph of spherical  $\text{UO}_2$  particles, about  $250 \mu\text{m}$  diameter, coated with pyrolytic carbon. The appearance of a "Maltese Cross" is due to optical anisotropy of the polished surface viewed under polarized light. (See "Fabrication of Coated Particle Fuel" by R.K. Rondeau and H.R. Lee.)



**MATERIALS RESEARCH IN  
ATOMIC ENERGY OF CANADA LIMITED**

FALL 1972

# CONTENTS

	Page
1. FABRICATION OF COATED PARTICLE FUEL .....	2
R.K. Rondeau and H.R. Lee Applied Science Division, WNRE	
2. STRESS-CORROSION CRACKING OF ZIRCONIUM ALLOYS .....	7
B. Cox Chemistry and Materials Division, CRNL	
3. STRESS-CORROSION CRACKING OF ZIRCONIUM ALLOY FUEL ELEMENT SHEATHS IN IODINE VAPOUR .....	13
J.C. Wood Fuels and Materials Division, CRNL	
4. DISTRIBUTION OF ZIRCONIUM HYDRIDE IN ZIRCALOY .....	16
J.F.R. Ambler Fuels and Materials Division, CRNL	
5. CRYSTAL DEFECTS STUDIED BY INTERNAL FRICTION .....	19
I.G. Ritchie Chemistry and Materials Science Division, WNRE	
6. TECHNIQUES TO STUDY TRANSPORT PHENOMENA IN ANODIC OXIDES ..	23
F. Brown Chemistry and Materials Division, CRNL	

WNRE           Whiteshell Nuclear Research Establishment  
                  Pinawa, Manitoba

CRNL           Chalk River Nuclear Laboratories  
                  Chalk River, Ontario

# FABRICATION OF COATED PARTICLE FUEL

Nuclear fuel consisting of small fissile particles dispersed in graphite is attractive for special applications. A three-stage process for fabricating this fuel is described.

The provision of excess reactivity to overcome the effects of fission product "poisons" allows CANDU power reactors to be returned to power rapidly after a shut-down. This reactivity is provided by inserting concentrated fissile material, contained in "booster assemblies", into the reactor core. To ensure efficient use of neutrons and good fission product retention a graphite-matrix dispersion-type fuel has been developed for booster applications. Small spheres (ca. 250  $\mu\text{m}$  diameter) of  $\text{UO}_2$ , coated with multiple layers of a semi-permeable pyrocarbon, are dispersed in graphite-matrix pellets which are then sealed in metal sheaths (see cover photograph). With a single fuel element consisting of a large number of individually coated particles, several coating failures may be tolerated without serious contamination of the coolant even if the sheath were to be ruptured.

## Microsphere Fabrication

A sol-gel process has been selected for fabricating microspheres, since it is suitable for large-scale automatic production.

$\text{UO}_2$  sols are prepared by the precipitation of hydrous U(IV) oxide and its subsequent filtration, dispersion and peptization. Figure 1 illustrates an engineering-scale flow sheet for preparing concentrated stable sols. The reduction and all subsequent handling and storage are carried out under an inert atmosphere as the presence of excessive concentrations of the U(VI) ion results in a precipitate which will not peptize.

After the U(IV) hydrous oxide is precipitated, washing reduces the ionic concentration of the precipitate to the point at which incipient peptization occurs. The precipitate is then transferred to a closed vessel and peptized in an ultrasonic bath operating at a frequency of 80 kHz. Distilled water is used as the

coupling medium and this, together with the precipitate, is self-heated to approximately 60°C. The peptization process is monitored, again by measuring the conductivity of the sol. These sols are quite stable, having a shelf life of several months.

Gel spheres are formed in a tapered glass column which is based on a design from the Oak Ridge National Laboratory in the USA. The equipment flowsheet is illustrated diagrammatically in Figure 2. The sol is fed from a constant flow syringe pump to an injection nozzle mounted coaxially in a tube with the solvent flowing downward past the jet. The droplet size is controlled by: feedrate, flow rate of solvent past the jet and the size of the injection nozzle. The droplets are fluidized in the column by a recirculating upflowing stream of an alcohol, 2-ethyl-1-hexanol. As the water is extracted and the droplets gelled, the settling velocity of the particles increases. The configuration of the column and the fluidizing flow rates are selected so that the gelled microspheres drop out continuously into a product collector at the bottom of the column at roughly the same rate that sol drops are being formed at the top of the column.

Agglomeration of the spheres in the column is prevented by the addition of surface active agents, the gelation time varying from  $6 \times 10^2$  to  $2 \times 10^3$  s according to sol concentration and droplet size. It is necessary to control the rate at which water is removed from the spheres by adjustment of the initial water content of the hexanol. When the rate of water removal is excessive (virgin alcohol) the different sizes of spheres produced sinter to different densities due to the increase in macroporosity in the centre of the larger spheres. Uniform density and sphere size, see Figure 3, is obtained by using hexanol containing initially 25% of the amount of water required for saturation.

The partially dried microspheres are fired in high

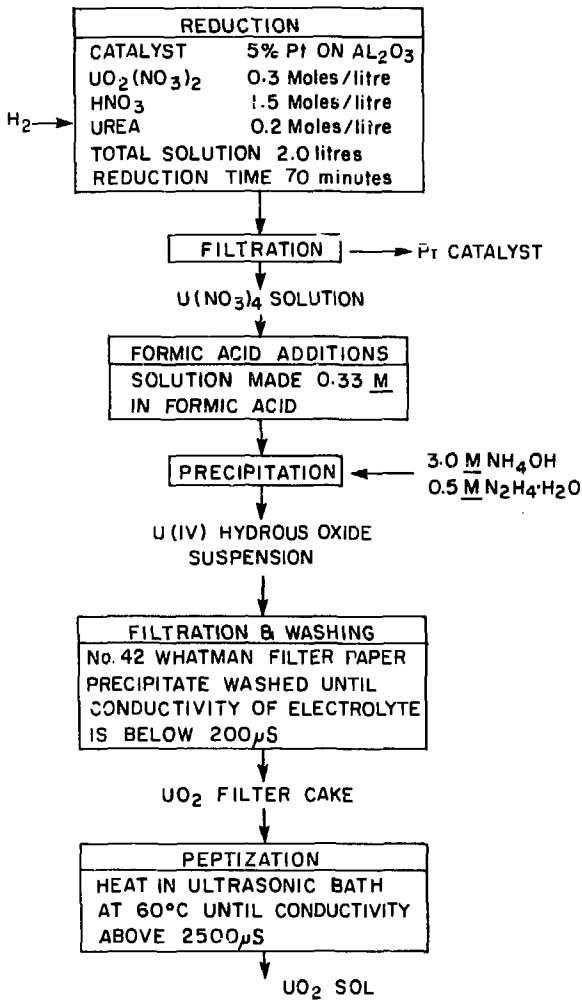


Figure 1 Preparation of format sol.

purity aluminum boats. The firing cycle is necessarily complicated and lengthy due to the need to remove all traces of water and alcohol before sintering of the outer surface of the microspheres commences. The cycle involves heating to 800°C in a steam/hydrogen mixture over a period of  $5.8 \times 10^4$  s and holding at a temperature of 1400°C for  $1.4 \times 10^4$  s. Typical microspheres are reproduced in Figure 4.

### Coating Techniques

A tubular fluidized bed coating furnace, typical of those used in pyrocarbon deposition, is contained within a Vycor tube. The tube and coating assembly are mounted coaxially inside the coils of an RF induction heater. The lower end of the bed, which also acts as the susceptor, terminates in a cone with a nozzle at its apex through which the fluidizing gas passes into the coater. The fluidizing gas, helium, levitates the particles while the pyrocarbon is deposited on them as a result of the high temperature pyrolysis of the coating gas. A wide range of hydrocarbons has been employed in the latter capacity, the identity of this gas, as well as its concentration, temperature and flow determining the characteristics of the pyrocarbon.

The coating of fuel particles serves a dual purpose, as a diffusion barrier and pressure vessel, since in preventing the escape of fission product gases it must be able to contain them against a steadily increasing internal pressure as the fuel is burnt up. A secondary function is to absorb recoiling fission fragments from the fuel kernel without suffering serious damage. A

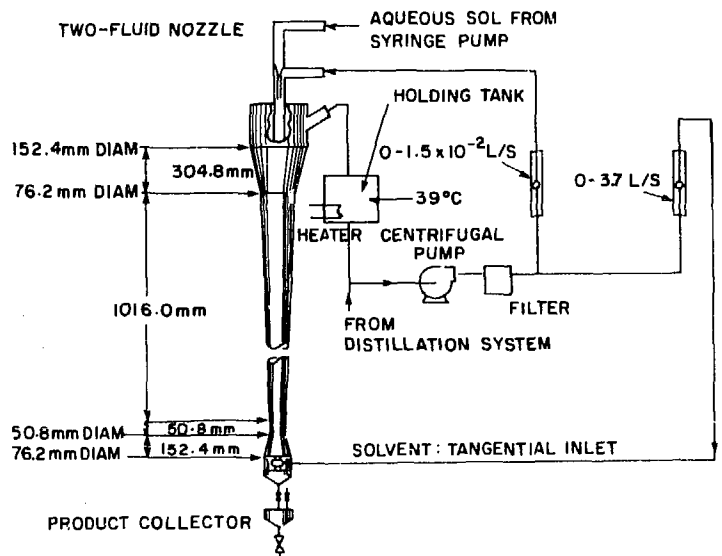
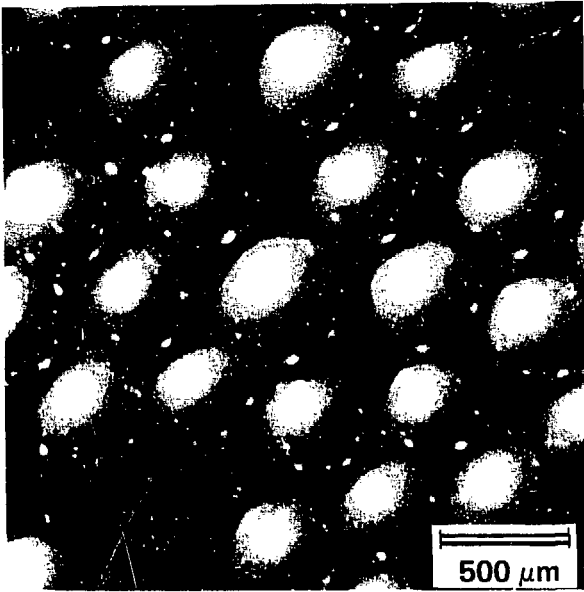


Figure 2 Schematic diagram of microsphere forming apparatus.



**Figure 3** Partially dried microspheres as removed from the forming column.

consequence of these various requirements has been the gradual evolution of monolithic pyrocarbon coatings into more complex structures, with successive layers having different characteristics and serving different functions as illustrated in Figure 5.

An inner sacrificial layer of relatively low density pyrocarbon is included in all coatings to accommodate the severe damage expected from fission recoils. This coating, deposited from acetylene at 1100°C, has a density of approximately 1.0 g/cm<sup>3</sup>. It provides an additional volume for fission gas, serves to absorb kernel swelling and protects the outer coating against uranium migration under irradiation. A second, outer pyrocarbon layer, constituting the pressure vessel, is deposited from propylene under

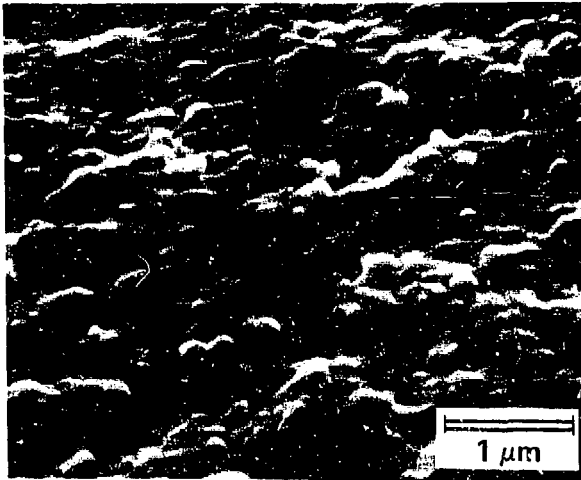
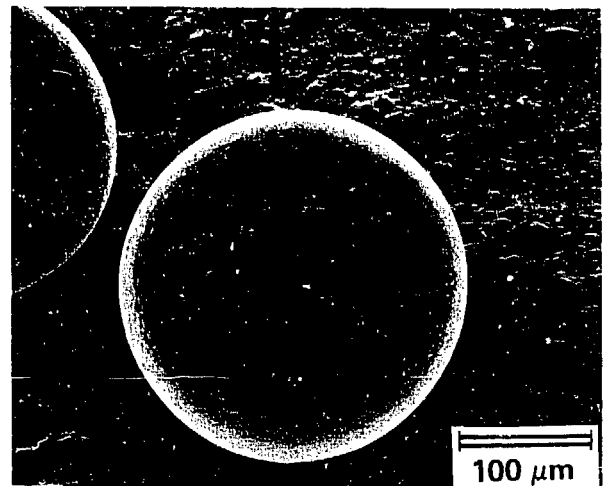
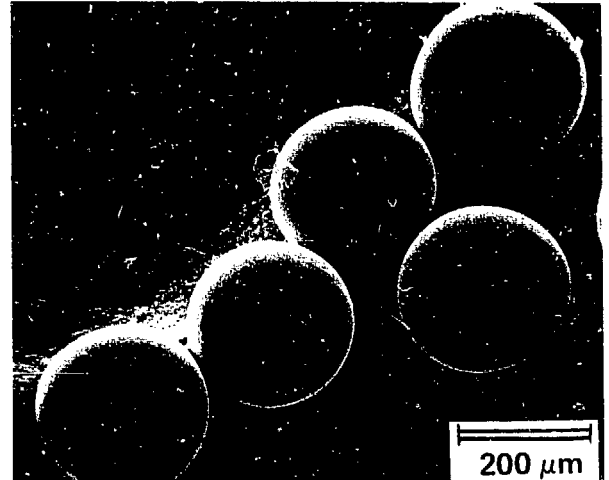


**Figure 4** Surface appearance of typical dried microspheres. Note the sphericity and smooth surface finish.



- (a) SURFACE OF FUEL KERNEL
- (b) INNER LOW DENSITY COATING
- (c) OUTER HIGH DENSITY PRESSURE VESSEL

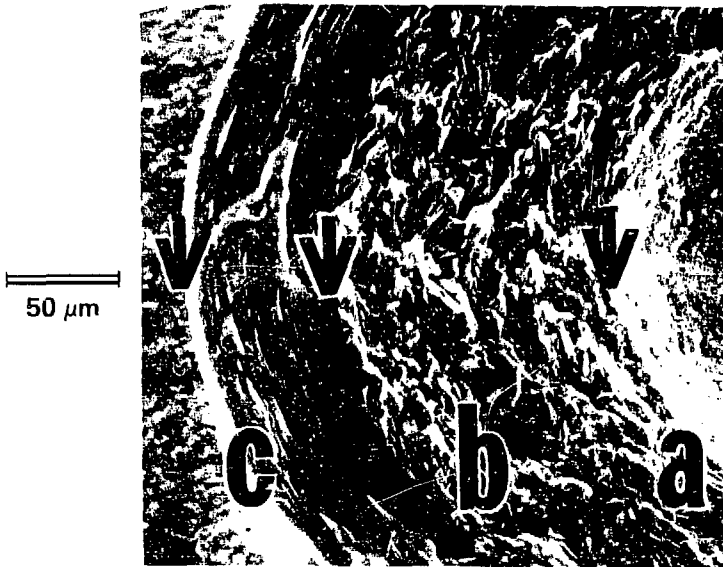


Figure 5 Cross section of finished coated particle.



Figure 6 Neutron radiograph of finished fuel element illustrating the excellent dispersive effect of the fabrication procedures adopted.



conditions to produce a density of approximately 1.8 g/cm<sup>3</sup>.

Although coatings have evolved into rather complex structures involving layers of widely varying composition, their deposition is carried out in a single furnace operation in which bare kernels are introduced at the start and completely coated particles are extracted from the bed at the end. Changes in temperature and the nature, flow rates etc., of the coating and fluidizing gases produce the required variation in properties in a continuous program.

### **Pellet Fabrication**

Fuel bodies are cold pressed by incorporating the coated particles with graphite flour and an appropriate resin binder. In an elegant method of doing this, the microspheres are covered with a coating of

resinated graphite powder, poured into a die of the correct shape and size and pressed into a compact at a pressure of 175 MN/m<sup>2</sup>. The green compact is subsequently aged at room temperature and heat treated to cure and carbonize the resin. This method yields a uniform distribution of particles (Figure 6), reduces particle damage during fabrication and produces an isotropic compact having a high thermal conductivity, calculated to be about five times that of a loosely bonded bed.

Judicious selection of a diameter for the forming die produces a finished pellet that is within the normal dimensional tolerances applicable to booster fuel fabricated via more conventional routes. Grinding and further fabrication procedures are thus not necessary before the fuel is assembled in stacks for encapsulation.

R.K. Rondeau & H.R. Lee

\*

# STRESS-CORROSION CRACKING OF ZIRCONIUM ALLOYS

The environments causing SCC of zirconium alloys are reviewed and the nature of the cracking process in each environment summarized.

Although stress-corrosion cracking (SCC) of titanium alloys has been known to occur in many environments for a considerable period of time, little work has been reported on the metallurgically similar zirconium alloys<sup>(1-4)</sup>. This may, in part, be due to the far more restricted range of environments in which zirconium alloys have been commercially exploited. In the chemical industry titanium is used, because of its lower cost, to the almost complete exclusion of zirconium and it is only in nuclear reactors, where savings in parasitic neutron absorption may be more important in the overall economics of the system than the initial cost of the material, that zirconium alloys have seen extensive commercial use.

As a result of the different situations in which titanium and zirconium alloys are used, the latter have seen exposure to only a limited number of environments which could potentially lead to SCC failures. However, with experience, the situations in which zirconium alloys are being employed in nuclear reactors are expanding beyond the traditional uses as fuel cladding and in-core structural components (e.g. pressure tubes), and the possibilities of encountering environmentally induced failures are correspondingly increased.

The environments known to crack titanium alloys (Table 1) have been examined at CRNL<sup>(5)</sup>, and at least one of each major group of these environments

has been shown to cause cracking of zirconium alloys. The conditions under which zirconium alloys are known to crack are summarized in Table 2 together with a brief description of the type of cracking, and possible situations in which this type of cracking might be encountered.

In situations where in-service failures occur, however, it may not be immediately obvious what the environment causing the failure was, since the conditions necessary for cracking may be only transient and result from maloperation or malfunction somewhere else in the system. As a clue to the cause of the failure, fractography can be very useful and Figure 1 shows that the characteristics of the fracture face produced in the environments studied at CRNL can be sufficiently diverse to have some diagnostic importance. However, under service conditions the presence of other factors (such as cyclic stressing) contributing to the failure could distort the fractography sufficiently to make identification of the cause of failure more difficult.

In addition to an environment capable of causing cracking, the metallurgical condition of the material, and the method of testing can be major influences in determining whether cracking occurs or not. More details of the manner in which these variables affect cracking in one environment ( $I_2$  vapour) are given in the next contribution to this issue of "Materials Research in AECL".

**Figure 1** Fractography by scanning electron microscope of low-nickel Zircaloy-2 fuel cladding (Batch ML 1-788) in;

- (a) Methanol/iodine
- (b) Methanol/HCl
- (c) Aqueous sodium chloride
- (d) Mercury
- (e) LiCl/KCl eutectic at 350°C
- (f)  $\text{KNO}_3/\text{NaNO}_3/\text{KI}$  at 300°C
- (g)  $\text{I}_2$  at 300°C

(a)–(d) were at room temperature.

Note presence of striations only in R T transgranular failures. Cleavage features occur on all transgranular fractures, but are severely etched in (b).

All fractographs 3,000X.



(a)



(b)



(c)



(d)



(e)



(f)



(g)

**TABLE 1. Environments in which some titanium alloys are known to crack (6,7)**

Type of environment	Temperature °C	Example
1. Organic liquids	RT	Methanol and solutions with I <sub>2</sub> , Br <sub>2</sub> , HCl, KBr, KI, NaBr, NaCl, CH <sub>3</sub> OH, H <sub>2</sub> SO <sub>4</sub>
	RT	Higher alcohols with similar additives
	RT	Ethylene Glycol
	300 – 800	Chlorinated Hydrocarbons (e.g. methylchloroform, CCl <sub>4</sub> , trichlorethylene, chlorinated diphenyl—“Aerochlor 1262”)
	RT	
	RT	Freons (e.g. Freon PCA, Freon TF, Freon MF, Freon C318)
2. Aqueous chloride solutions	RT	Hydrochloric acid (10%) NaCl, KCl, KBr, MgCl <sub>2</sub> , CuCl <sub>2</sub>
	25 – 154	
3. Hot and fused halide salts	300 – 450	NaCl, KCl, KCl/LiCl, KBr/LiBr, AgCl, MgCl <sub>2</sub> , SnCl <sub>2</sub> , CsCl, CaCl <sub>2</sub> , SrCl <sub>2</sub> , BaCl <sub>2</sub>
	300 – 450	Dried “sea-salt”
	350	KNO <sub>3</sub> /NaNO <sub>3</sub> /KI
	350	LiNO <sub>3</sub> /KNO <sub>3</sub> /KCl
	350 – 400	Cl <sub>2</sub> , HCl
5. Liquid metals	RT & 400	Mercury, cadmium, cesium, zinc
6. Solid metals	300	Cadmium
	450	Silver
7. Oxides and oxy-acids of nitrogen	RT	N <sub>2</sub> O <sub>4</sub>
	RT	Red fuming nitric acid
8. Miscellaneous	RT	Sulphuric acid
	0	Hydrogen gas
	RT	Methanol vapour

TABLE 2. Environments shown to cause cracking of zirconium alloys

Type of Environment and possible occurrence	Temperature °C	Example	Remarks
Organic Liquids – Use of organic cleaning liquids, or of organic liquids in tests simulating high temp. water	RT	Methanol and solutions with Br <sub>2</sub> , I <sub>2</sub> , NaCl	Intergranular; unstressed specimens degraded
	RT	Methanol/HCl	Initiation intergranular, propagation transgranular. Unstressed specimens attacked but not disintegrated.
	RT	Freon 11	Precracked specimens only
	RT	Methanol and solutions with H <sub>2</sub> SO <sub>4</sub> , HCOOH <sup>(1)</sup>	
	RT	Ethanol/HCl <sup>(1)</sup>	
Aqueous chloride solutions – Leaching of chlorides from valve packing or concentration of leaks could give suitable environment	RT	NaCl (0.01 – 5%) <sup>(10)</sup>	Predominantly transgranular. Requires anodic polarization beyond oxide breakdown potential. May be achieved by galvanic coupling to Pt if pre-oxidized.
	RT	FeCl <sub>3</sub> <sup>(3,4)</sup> , CuCl <sub>2</sub> <sup>(11)</sup>	Intergranular
	300°C	NaCl <sup>(11)</sup>	No tests yet at CRNL
Hot and fused salts – dry-out conditions in-reactor may lead to accumulation of salt deposits if prolonged times are involved. Nitrate ion could come from radiolysis of ammonia	300 – 350	NaCl, LiCl/KCl, CsI	Predominantly transgranular, appears to be initiated by cracking of protective oxide film
	300	KNO <sub>3</sub> /NaNO <sub>3</sub> /KI(KBr)	
	300	KNO <sub>3</sub> /NaNO <sub>3</sub> /KCl	Severe intergranular penetration with internal oxidation. Has been observed in leaking in-reactor autoclave tests <sup>(8,9)</sup> .
Halogen and halogen acid vapours – Iodine is a common fission product in irradiated fuel	RT	Cl <sub>2</sub> , Br <sub>2</sub> , I <sub>2</sub>	Predominantly transgranular. Crack velocity is slowest in Cl <sub>2</sub> . Requires precracked specimens.
	250 – 400	I <sub>2</sub> (+O <sub>2</sub> or Fe)	No precrack required, but needs O <sub>2</sub> or Fe as "catalyst". Metallurgical variables important. Predominantly transgranular.
Liquid metals – Cesium is a major fission product in irradiated fuel	RT	Mercury, cesium	Requires dynamic loading and good wetting. Transgranular.

All the zirconium alloys in common use appear to be susceptible if in the right metallurgical condition, although in some environments this is not critical. In general, as progress towards higher-strength zirconium alloys is made, one would expect a trend towards greater susceptibility to SCC such as is observed with the high strength titanium alloys.

B. Cox

## REFERENCES

1. K. Mori, A. Takamura and T. Shimose, *Corrosion*, 22 (1966) 29.
2. H.S. Rosenbaum, *Electrochem. Tech.*, 4 (1966) 153, and U.S. Report GEAP 5100-5 (1966).
3. J.T. Dunham and H. Kato, U.S. Report BM-RI-5784 (1961).
4. K.C. Thomas and R.J. Allio, *Nucl. Appl.*, 1 (1965) 252.
5. B. Cox, *Corrosion*, 28 (1972) 207.
6. Proceedings of Conference on "Fundamental Aspects of Stress Corrosion Cracking", Ed. Staehle, Forty and van Rooyen, NACE (1969).
7. M.J. Blackburn, J.A. Feeney, T.R. Beck, "Stress Corrosion Cracking of Titanium Alloys", Boeing Scientific Research Labs. U.S. Report D1-82-1054 (1970).
8. B. Cox, *Oxidation of Metals*, 3 (1971) 399.
9. B. Cox, U.K.A.E.A. Report AERE C/R 2826 (1959).
10. B. Cox, *Corrosion*, to be published.
11. R.L. Cowan, G.E. Vallecitos, private communication.

\*

# STRESS-CORROSION CRACKING OF ZIRCONIUM ALLOY FUEL ELEMENT SHEATHS IN IODINE VAPOUR

Metallurgical factors influencing SCC of zirconium alloys in iodine vapour are described, and a possible model for cracking of fuel element sheaths is given.

Iodine vapour induces transgranular and intergranular cracking of zirconium alloys when they are stressed in tension<sup>(1-3)</sup>. The subject is of interest because iodine is an abundant fission product and tensile stresses arise in fuel element sheaths due to thermal expansion of the UO<sub>2</sub> fuel pellets during irradiation.

Rings of zirconium alloys cut from sheath tubes were split longitudinally on one side and opened on zirconium wedges to produce a tensile stress at the inner surface. The stressed slotted rings were sealed with known amounts of iodine crystals in Pyrex capsules from which air and moisture had been evacuated. Then they were heated to temperatures experienced by fuel sheathing. This simple technique has enabled evaluation of many metallurgical and environmental variables including applied stress, residual stress, crystallographic texture, surface condition, cold work, irradiation hardening, temperature, iodine concentration, and the presence of catalysts — notably iron and air.

In order for stress-corrosion cracks to nucleate and grow, three conditions must be satisfied, viz. a susceptible alloy by virtue of its chemical composition and metallurgical structure, stresses exceeding some

critical stress, and a (mildly) aggressive chemical environment. The alpha-phase zirconium alloys tested were Zircaloy-2\*, Zircaloy-4†, Zr-2.5 wt% Nb, and Zr-1.25wt%Cr-0.1wt%Fe. All have the hexagonal close-packed structure which is susceptible to transgranular SCC and all will crack in iodine vapour in some metallurgical conditions. The iodine concentrations in which Zircaloy-2 rings have been cracked and the resultant times to failure are shown in Figure 1.

The critical stress for stress-corrosion cracking (SCC) can be achieved when the yield strength of an alloy is high (e.g. work hardened or irradiation hardened) or when a high residual tensile stress in the material combines with the applied tensile stress. In the fully annealed condition none of the alloys mentioned above is susceptible to SCC in iodine but after irradiation in a fast neutron flux of  $5 \times 10^{24}$  n/m<sup>2</sup> (E>1MeV) all will crack. Cold work causes Zr-2.5 wt% Nb to fail more readily than the other alloys because it work hardens to higher strength. All the results shown in the figures were obtained using a batch of Zircaloy-2 with a high residual tensile stress at its inner surface. It was demonstrated that residual stress can be more important than cold work in

---

\* Zircaloy-2 = Zr-1.5wt%Sn-0.2wt%Fe-0.1wt%Cr-0.05wt%Ni.

---

† Zircaloy-4 = Zr-1.5wt%Sn-0.2wt%Fe-0.1wt%Cr.



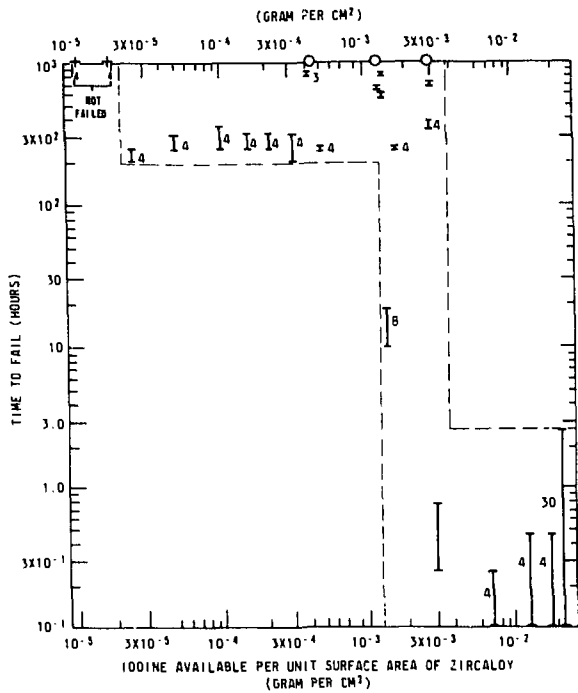


Figure 1 Dependence of time to fail on iodine concentration for Zircaloy-2 rings with an initial applied stress of  $310 \text{ MN/m}^2$  (45 kpsi).

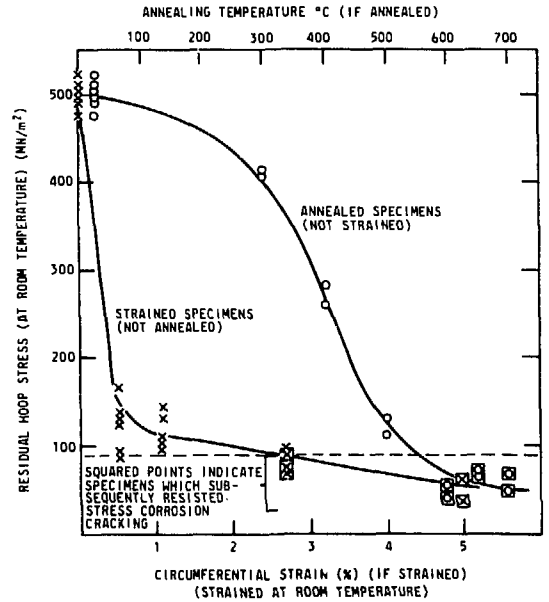


Figure 2 Removal of tensile residual stress increases stress-corrosion resistance.

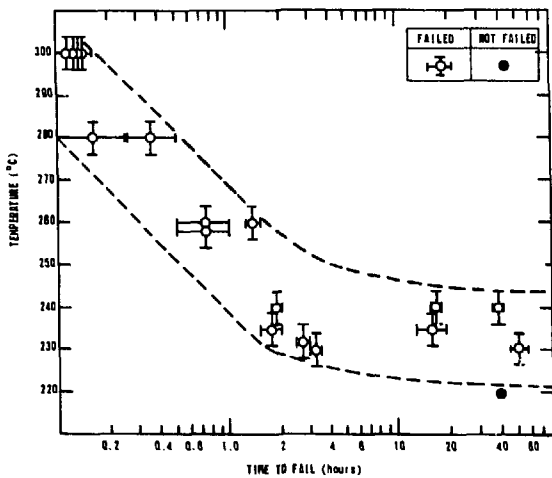


Figure 3 Variation of time to fail with temperature at a given applied stress ( $310 \text{ MN/m}^2$ ) and iodine concentration ( $3 \times 10^{-3} \text{ g per cm}^2 \text{ Zr surface}$ ).

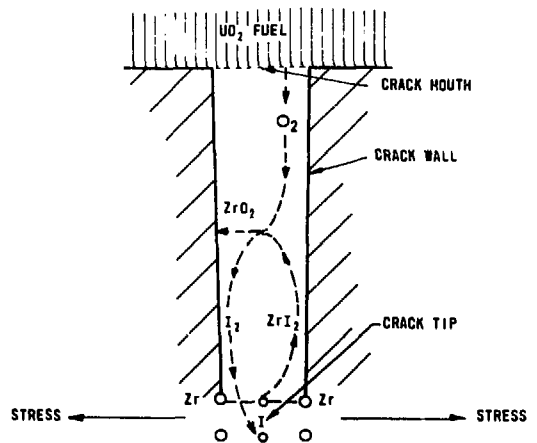


Figure 4 Possible mechanism for stress-corrosion cracking of zirconium alloy fuel sheaths in iodine vapour in which iodine is recycled within the crack.

determining susceptibility to SCC by removing the residual stress in two different ways:

- (1) by annealing – which also decreased cold work, and
- (2) by hydraulically straining – which increases cold work while removing residual stress.

The results of the experiment, given in Figure 2, show that specimens resisted SCC when stressed to the yield point in 300°C iodine vapour if the residual stress had been removed.

Crystallographic texture had no strong influence on susceptibility to SCC but it did affect crack direction. In tubes with basal poles preferentially circumferential, cracks were almost straight and radial whereas radial basal poles gave rise to branching cracks oriented about 45 degrees from the radial direction. Thus cleavage on or near the basal plane is a likely fracture mode.

Times to failure of stressed Zircaloy-2 rings increased strongly with decreasing temperature in the range of 300-220°C (Figure 3). It is known<sup>(2)</sup> that tubular specimens of Zircaloy-2 stressed by thermally expanding mandrels will fail up to 510°C. Fast<sup>(4)</sup> has shown that the chemical reaction rate between zirconium and iodine in the van Arkel<sup>(5)</sup> process is a maximum at 300°C and decreases to about 70% of the maximum at both 220 and 510°C. This coincidence suggests a possible model for the SCC of fuel sheaths involving very small quantities of iodine. If a volatile zirconium iodide formed at the crack tip it could migrate up the temperature gradient to either decompose thermally or release iodine by reaction with oxygen from the UO<sub>2</sub> fuel. Zirconium oxide

could then be deposited on the crack walls passivating them to localize further attack at the crack tip (Figure 4).

Several ways of preventing SCC of zirconium alloy fuel sheaths by iodine have resulted from these studies and some have already been demonstrated in-reactor. These may be the subject of a future review, subject to the results of current patent applications.

J.C. Wood

## REFERENCES

1. H.S. Rosenbaum, *Electrochem. Tech.* 4 (1966) 153.
2. A. Garlick and P.D. Wolfenden, *J. Nucl. Mat.* 41 (1971) 244-292.
3. J.C. Wood, to be published in *J. Nucl. Mat.* (1972).
4. J.D. Fast, *Z. Anorg. u. Allgem. Chem.*, 239 (1938) 145.
5. A.E. van Arkel and J.H. de Boer, *Z. Anorg. Chem.* 148 (1925) 345.

\*

# DISTRIBUTION OF ZIRCONIUM HYDRIDE IN ZIRCALOY

In slowly cooled Zircaloy the amount of intergranular hydride is a linear function of the hydrogen concentration. Below approximately 423 K (150°C) all the hydride is precipitated at the grain boundaries. The orientation frequency of the intragranular hydride is a non-linear function of the hydrogen concentration.

Zirconium is a member of the group of metals which form solid hydrides. At ambient temperatures hydrogen has negligible solubility in zirconium and in slowly cooled material it is present as well developed hydride plates. These are brittle at room temperature and, depending upon their degree of orientation relative to the stress system, can drastically reduce the strength and ductility of zirconium alloys<sup>(1)</sup>. At temperatures above 423 K (150°C) zirconium hydride is ductile and has little effect on mechanical properties<sup>(2)</sup>.

In polycrystalline zirconium alloys the hydride plates are both intergranular and intragranular (Fig. 1). Since intergranular hydride may have a greater effect on mechanical properties than intragranular hydride, we have measured the relative amounts of the two forms in annealed, slowly cooled Zircaloy\*.

Specimens from six batches of reactor fuel sheathing, covering a range of hydrogen concentrations, were examined.

For the specimens with grain sizes in the range 12 to 55  $\mu\text{m}$ , the volume fraction of the intergranular hydride was:

- independent of grain size and crystallographic texture.
- inversely dependent upon hydrogen concentration up to approximately 200 ppm, above which it was virtually constant (Fig. 2).

The amount of intergranular hydride, expressed as the hydrogen concentration present as grain

\* A zirconium-rich alloy containing 1.5 wt% Sn, 0.2 wt% Fe and 0.1 wt% Cr.

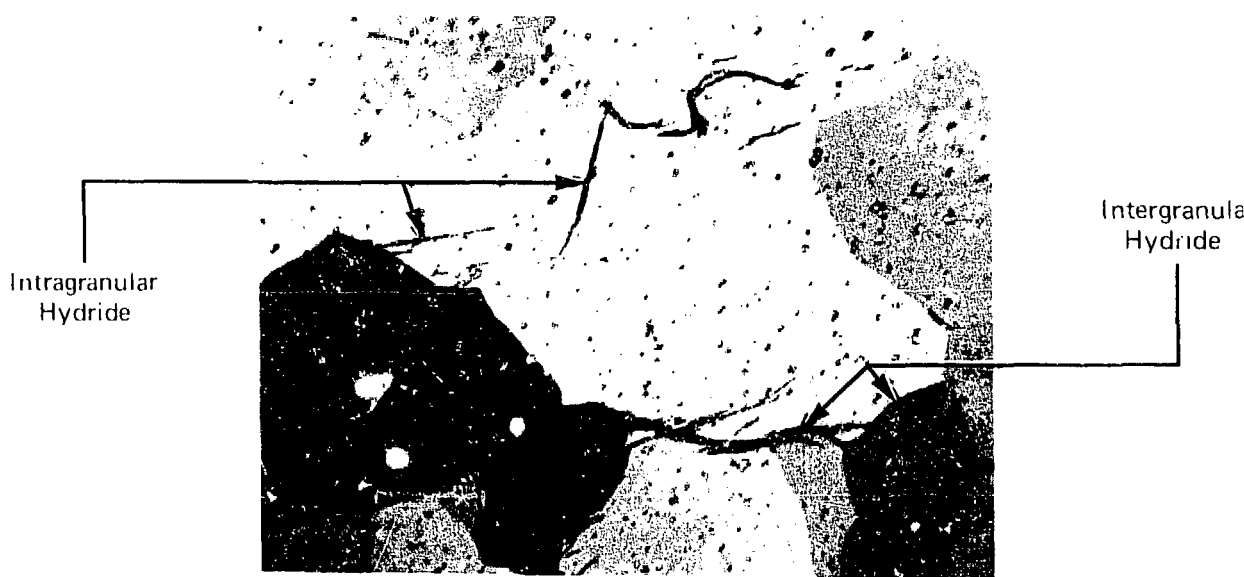


Figure 1 Inter- and intra-granular hydride plates in annealed Zircaloy containing 123 ppm hydrogen. Polarized light (500 X).

boundary hydride, was directly proportional to the total hydrogen concentration (Fig. 2). The slope of the line is about 0.5.

Extrapolation of the linear relationship (Fig. 2) indicates that at hydrogen concentrations less than 25 ppm, all the hydride would be at the grain boundaries. The form of the relationship can be explained if, during cooling, inter- and intra-granular hydride precipitate in equal amounts until the temperature reaches 423 K (150°C), after which the last 25 ppm precipitates exclusively at the grain boundaries.

Using other specimens, we were able to demonstrate experimentally that the last 25 ppm hydrogen, i.e. below 423 K (150°C), did precipitate at the grain boundaries but prior to this more inter- than intra-granular hydride was formed (Fig. 3). The reason for this difference from previous results is probably the fine grain size of the new specimens (8  $\mu\text{m}$ ) compared to that of those used in the initial experiments (12 to 55  $\mu\text{m}$ ). This indicates that for grain sizes less than approximately 10  $\mu\text{m}$ , the volume fraction of intergranular hydride increases with decrease in grain size. The fraction would probably decrease with increase in grain size for coarse grained material.

Grain boundary stresses, resulting from the anisotropic contraction of the individual zirconium grains during cooling, are thought to be the reason why the last 25 ppm hydrogen precipitates exclusively at the grain boundaries. These stresses would become significant only at a temperature where the rate of stress increase was greater than the rate of

stress relaxation. This temperature will depend upon the cooling rate and for our experimental conditions appears to have been about 423 K (150°C). There is no direct evidence that these stresses cause grain boundary segregation of hydride. However, Roy suggested that such stresses could be the reason why low temperature annealing at 353 K (80°C) of previously quenched zirconium specimens results in

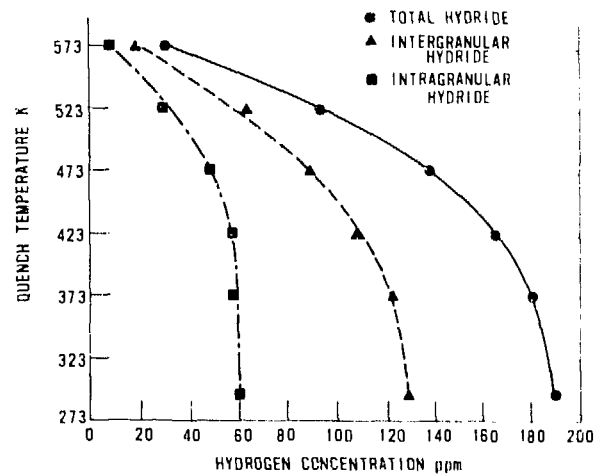


**Figure 3** Zircaloy specimens, containing 190 ppm hydrogen, were slowly cooled from 1073 K (800°C) and quenched from the temperatures shown. The curves indicate how the hydride, precipitated between the solid solubility temperature and the quench temperatures, was distributed between inter- and intra-granular forms.

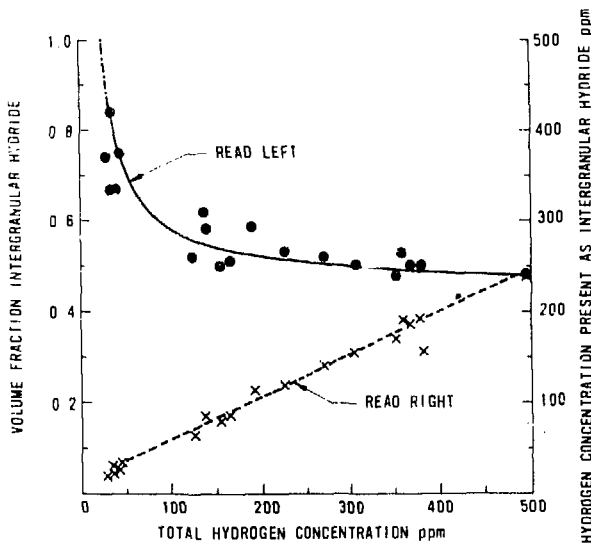


**Figure 2** Fraction and amount of intergranular hydride as a function of total hydrogen concentration in annealed Zircaloy.

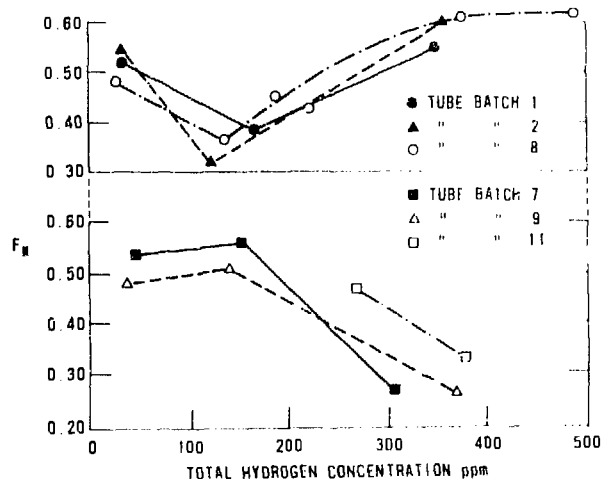


**Figure 4** Orientation frequency of intragranular hydride ( $F_N$ ) as a function of total hydrogen concentration for six batches of Zircaloy tubing.

almost complete segregation of the hydride at the grain boundaries<sup>(3)</sup>.

Measurements of the orientation of the two forms of hydride, expressed as the frequency,  $F_n^*$ , showed that:

- $F_n$  for the intergranular hydride was independent of the hydrogen concentration.
- $F_n$  for the intragranular hydride was a maximum or minimum at hydrogen concentrations between 50 and 150 ppm, depending upon the particular fuel sheathing batch (Fig. 4).

We were unable to explain these two observations but it follows that, qualitatively, the orientation frequency for the total hydride depends upon the hydrogen concentration in the same way as does the orientation frequency for the intragranular hydride.

---

\*  $F_n$  is the fraction of hydride plates lying within 0.698 rad ( $40^\circ$ ) of the radial direction of the tube as seen on a transverse section.

Thus hydride orientation is not simply a function of the fabrication process.

J.F.R. Ambler

## REFERENCES

1. R.P. Marshall, and M.R. Louthan, Trans. Am. Soc. Metals, 56 (1963) 693.
2. W. Evans, and G.W. Parry, Electrochemical Tech., 4 (1966) 225.
3. C. Roy, Atomic Energy of Canada Limited Report AECL-2297 (1965).

For more detailed information see:

J.F.R. Ambler, and P.G. Olson, Proc. International Congress "Hydrogen in Metals", Paris, May/June 1972, p. 474.

\*

# CRYSTAL DEFECTS STUDIED BY INTERNAL FRICTION

Internal friction measurements can give information on the interaction between dislocations and point defects. Results are given for single crystals of magnesium oxide.

## INTRODUCTION

Over the last fifteen years, the technique of internal friction has become well known as a tool for the investigation of dislocations and their interaction with point defects in crystalline solids<sup>(1)</sup>. A great many of the theoretical developments in the field of dislocation damping have originated from the Granato and Lüke (G - L) theory<sup>(2)</sup>. In the G - L model, the dislocation, under the action of an applied stress, behaves like a stretched string and bows out between pinning points. The dislocation is assumed to be strongly anchored at its extremities where stable nodes are formed with the dislocation network. At intermediate points, the dislocation is weakly pinned at local sites such as point defects. As the dislocation bows, the localized anelastic strain gives rise to dissipation of energy due to the scattering of thermal phonons. This energy is supplied by the mechanical system applying the stress and manifests itself as heat in the material which is transferred irreversibly to the surrounding environment. The magnitude of this dissipation is measured in an internal friction experiment where the attenuation of amplitude is measured in a freely vibrating specimen, energy being dissipated in each cycle. The measure of damping, the decrement, is expressed as the ratio of the energy dissipated per unit volume in one cycle to twice the maximum strain energy per unit volume realized in that cycle.

For low initial strain amplitudes, the damping is *independent* of the strain amplitude. However, as the initial strain amplitude is increased, a critical threshold stress is eventually reached where the dislocation breaks away from the weaker pinning points. The resulting sudden increment of anelastic strain results in a further contribution to the overall damping. As this strain increment is constant and invariant with

stress above the breakaway stress, the resulting damping contribution, as defined above, is *amplitude-dependent*, decreasing with stress because the maximum strain energy per cycle increases with amplitude.

Initially, this model met with a great deal of success in explaining the observed experimental results. The model continues to be successfully applied to experimental amplitude-independent data, but amplitude-dependent data, for many materials, cannot be explained on the basis of this model alone. This inconsistency can be attributed to the misapplication of a model, which is essentially a zero temperature description, to temperature regimes where dislocation breakaway is thermally assisted.

The study of damping that is dependent on strain amplitude yields information on both point defects and dislocations and their mutual interaction. It therefore intimately relates to the fields of plastic deformation and radiation damage and is, consequently, of considerable theoretical and technological interest. Further developments in this field of research have awaited a tractable theory of thermally assisted unpinning.

## THEORY OF THERMALLY ASSISTED UNPINNING

The first attempt at incorporating thermal activation into the G - L theory was made by Teutonico, Granato and Lüke (T-G-L)<sup>(3)</sup>. Their results, however, were too complicated to compare with experimental data. Recently, Blair, Hutchison and Rogers (B-H-R)<sup>(4)</sup> have incorporated a general pinning force into the T-G-L theory and with simplifying, yet justifiable assumptions, have made detailed calcula-

lations of the complex damping behaviour attributable to thermally assisted breakaway. They have shown that the results can be conveniently represented in a Temperature ( $T$ ) – Strain ( $\epsilon$ ) diagram. For very long dislocation loops, the  $T$ - $\epsilon$  diagram has given regions (A-E) of different damping behaviour, as shown in Figure 1. The corresponding damping versus strain amplitude curves are shown in Figure 2, where the positions of the boundaries between adjacent regions are indicated. Blair, Hutchison and Rogers have formulated theoretical expressions for these boundaries in terms of the dislocation loop length and the dislocation-pinner binding energy.

The five regions of the  $T$ - $\epsilon$  diagram are required to describe all the possible activated complexes of a dislocation with multiple pinners. Thus, in regions A and E, breakaway is activated over a group of pins, while in regions B, C and D, breakaway from the whole row of pinners is activated at a single pin. Regions A and B are characterized by few of the dislocations breaking away in a given strain cycle, whereas in regions C and E nearly all the dislocations breakaway in a given cycle. Region D, which is characteristic of very long loops, is different from all other regions in that the activation energy for un-

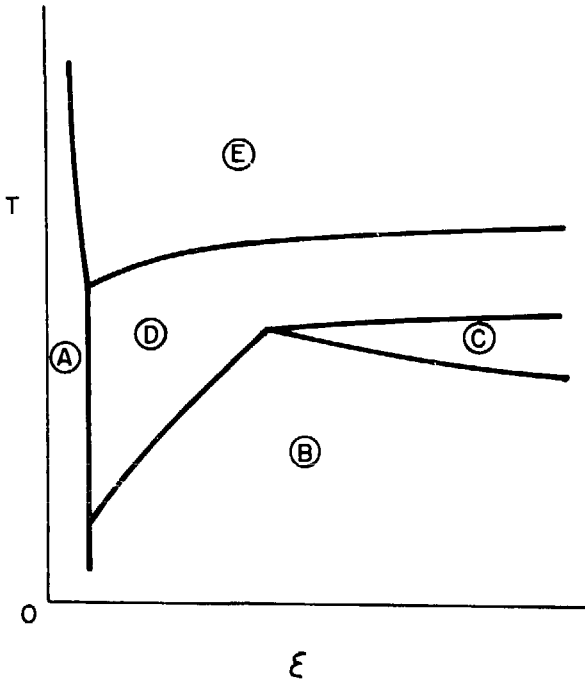


**Figure 1** Schematic diagram of the strain amplitude ( $\epsilon$ ) – temperature ( $T$ ) plane for very long loops [after Blair et al. (4)].

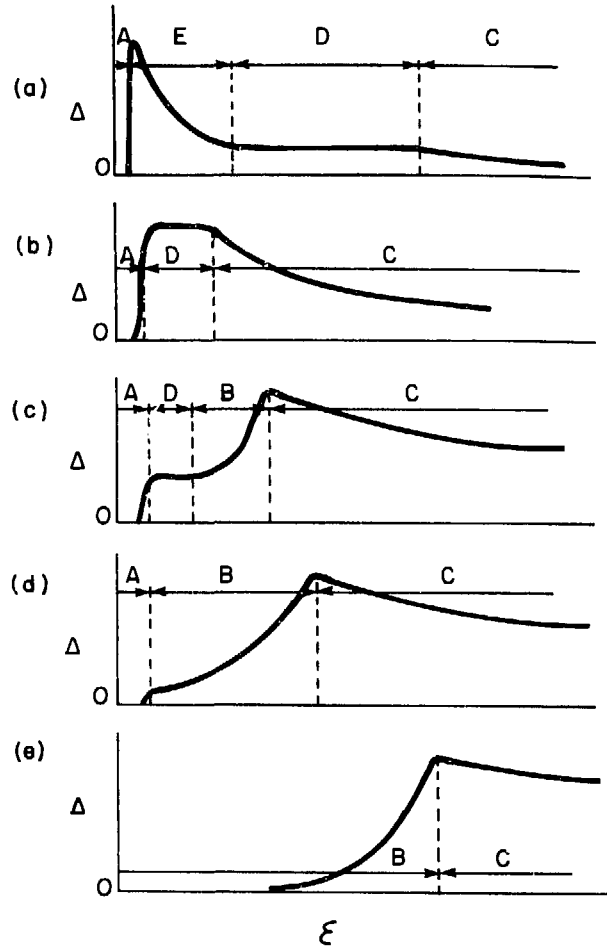


**Figure 2** Schematic curves of decrement ( $\Delta$ ) as a function of strain amplitude ( $\epsilon$ ) for very long loops used in constructing Fig. 1. The temperature decreases from (a) to (e) [after Blair et al. (4)].

pinning is effectively constant, during a given cycle.

Some of the theoretical prediction of the B-H-R theory can be tested quite readily by experiment and the self-consistency of the expressions for the critical strains checked. In addition, the most interesting predictions, which are for very long loops, can yield definitive information on the asymptotic behaviour of the law of force between dislocations and pinning points. The experiment should, therefore, be carried out on a material, such as MgO single crystals, in which fresh dislocations can be easily generated at temperatures where they are not rapidly pinned by diffusional processes. This, together with the fact that well annealed single crystals have a low intrinsic dislocation density, ensures the requirement of 'very long loops'.

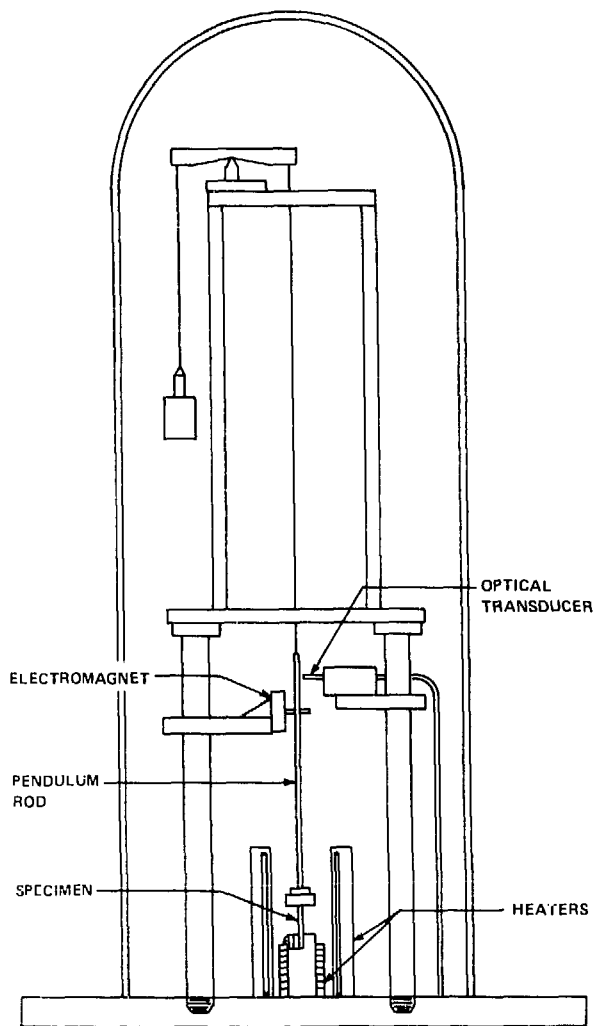


Figure 3 Counterbalanced reed pendulum.

## EXPERIMENTAL TECHNIQUE

Investigation of strain amplitude dependent damping requires an apparatus in which the strain amplitude and temperature can be controlled with accuracy and small changes in damping be accurately recorded. The counterbalanced reed pendulum shown schematically in Figure 3 meets these requirements. In principle, the operation of the pendulum is very simple. The specimen *S*, in the form of a rectangular prism, is clamped between grips fixed in the case and grips attached to the pendulum rod, *R*. Static compressive strains are removed from the specimen by carefully counterbalancing the assembly. Flexural vibrations of the pendulum are initiated by pulsing

the electromagnet *E* and the subsequent free decay in amplitude is monitored by the optical transducer *T*. This transducer is a fibre optical device which measures linear displacement with a sensitivity of about  $10^{-5}$  cm.

After curve-fitting the amplitude decay curve and applying a correction for the strain distribution in the specimen, the results can be compared with the B-H-R theory. Typical experimental curves are shown in Figure 4. These should be compared with the low strain portions of the theoretical curve (c) in Figure 2.

## RESULTS

A typical  $T$ - $\epsilon$  diagram for an MgO crystal that was neutron-irradiated then annealed is shown in Figure 5. All of the regions predicted by the B-H-R theory have been detected. Quantitative comparisons of our data with the B-H-R theory have generally shown good agreement. Calculation shows that, in our

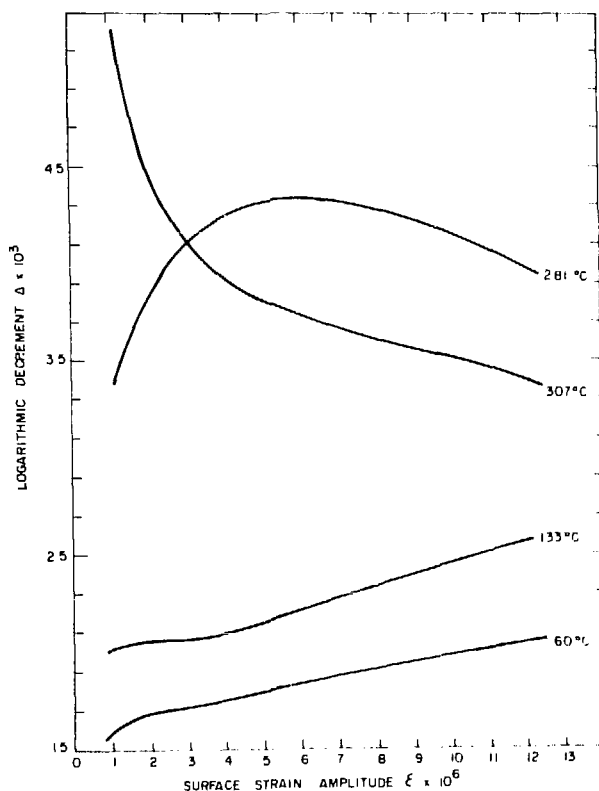


Figure 4 A selection of experimental curves of decrement as a function of strain amplitude for an MgO single crystal. Note the change in shape of the curves, with temperature and compare with the theoretical curves in Figure 2.



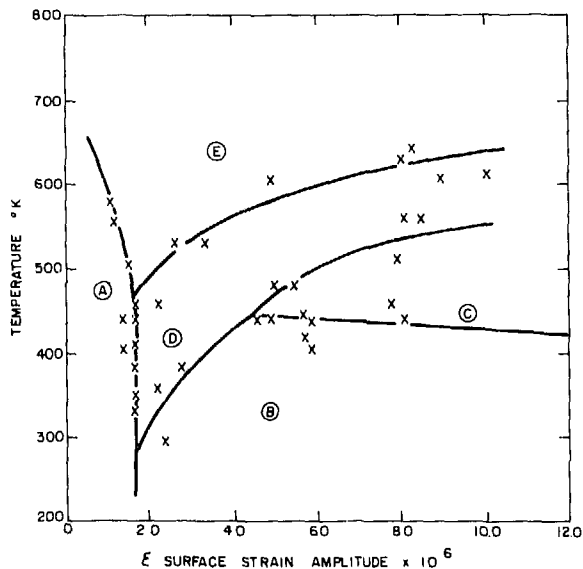


Figure 5 Strain amplitude - temperature diagram for a neutron irradiated and annealed single crystal of MgO. Compare with the schematic diagram Fig. 1.

specimens of MgO, the fresh dislocations have a loop length of about  $1 \times 10^{-4}$  cm and are pinned by a species of pinner having a binding energy to the dislocation of about 1 eV. There is some theoretical evidence to suggest that the pinner is the positive-ion vacancy, but this has not yet been confirmed.

## FUTURE EXPERIMENTS

In experiments on neutron-irradiated MgO single crystals, the cycle of shapes shown in Figure 2 has been observed to repeat several times in the temperature range, ambient to  $700^{\circ}\text{C}$ . This results in overlapping T- $\epsilon$  diagrams that are difficult to interpret. In addition, the thermally assisted breakaway mechanisms are probably accompanied by changes in damping due to rearrangement of the pins by core diffusion. However, the results indicate that there may be a whole spectrum of pinners of different strengths in the neutron irradiated material and that fresh dislocations can be effectively used as an internal friction probe to study the structural changes associated with radiation damage. Thus, further experiments on irradiated MgO are planned. Besides aiding in the identification of the species of pinners responsible (and hence the nature of the radiation induced point defects), a direct indication of their effect on mechanical properties and annealing characteristics should be possible from these experiments.

Internal friction is the only method at present

available which directly measures the interaction between dislocations and point defects. It is evident that the experimental approach presented here, in conjunction with other established techniques, presents the experimentalist with a new and powerful tool for the study of many aspects of radiation damage and mechanical properties.

I.G. Ritchie

## REFERENCES

1. C.F. Burdett and T.J. Queen, *Metallurgical Review* Number 143, Part II. Metals and Materials (1970).
2. A. Granato and K. Lücke, *J. Appl. Phys.*, 27 (1956) 583.
3. L.J. Teutonico, A.V. Granato and K. Lücke, *J. Appl. Phys.* 35 (1964) 220.
4. D.G. Blair, T.S. Hutchison and D.H. Rogers, *Can. J. Phys.* 49 (1971) 633.

For more detailed information see:

K.W. Sprungmann and I.G. Ritchie

"An Improved Reed Pendulum Apparatus and Techniques for the Study of Internal Friction of Ceramic Single Crystals" Atomic Energy of Canada Limited Report AECL-3794, 1971.

\*

# TECHNIQUES TO STUDY TRANSPORT PHENOMENA IN ANODIC OXIDES

Techniques have been developed to study whether anodic oxides grow by migration of oxygen, metal, or both and also to study the movement of foreign atoms in anodic oxides. These techniques could find applications in thermal oxidation, corrosion and investigations of their films in general.

In studies of transport phenomena the objective is often to determine whether, during oxidation of a metal, the oxide grows by migration of oxygen inwards through the oxide film, migration of metal outwards, or a combination of both. One may also want to find how these transport phenomena are affected by oxidising conditions. Techniques involving "inert markers" have proved invaluable in these experiments.

The basis of the methods is to introduce into the

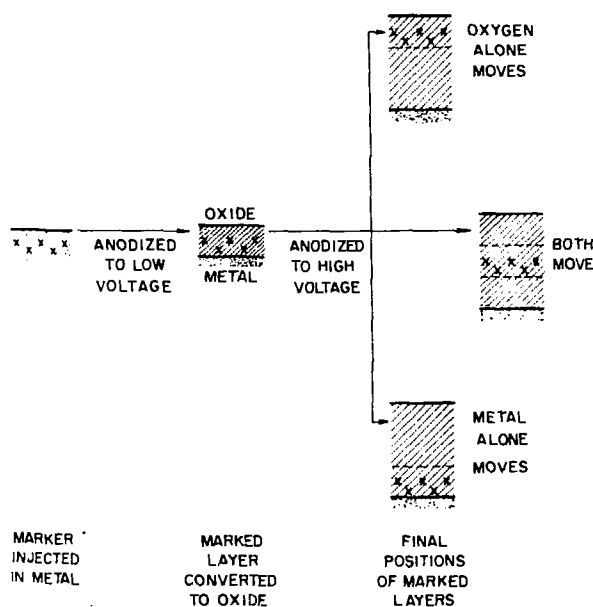


Figure 1 Diagram illustrating the possible fates of inert markers during oxidation.

metal surface an immobile 'marker' and then, after oxidation, determine whether the oxide has formed below the marker, above it, or both. Oxide formed below the marker has formed by inward migration of oxygen whilst oxide formed above the marker has formed by outward migration of metal (Figure 1). In practice, it is often preferable to introduce the marker into a thin oxide already grown on the metal and then grow more oxide. To make the experiments quantitative it is necessary, in either case, to measure both the thickness of oxide grown and the depth of the marker within it, or strictly speaking, the ratio of these two quantities.

For very thick oxides the marker could be a solid object such as a fine platinum wire. However, for thin oxides and specifically for anodically formed oxides, whose thickness does not exceed a few thousand Angstroms, this procedure is clearly impractical. One must now resort to introducing foreign atoms as markers and after oxidation one must locate their depth by some technique that has a resolution in the order of 100Å, or preferably less.

In all our work we have used atoms of the noble gases, argon, krypton, xenon or radon, as markers. They have been introduced into the metal, or preformed oxide, by ion bombardment. The electromagnetic isotope separator at CRNL is an ideal instrument since it can provide, when required, beams of isotopically separated radioactive tracers. A bombardment energy of 5 keV is typical; the range of such heavy ions is less than 50Å hence they form a narrow distribution, initially very close to the surface.

Techniques for measuring the depth of the markers after oxidation fall into two broad classes

the first of which depends upon controlled stripping of the oxide. A radioactive tracer, e.g.  $^{85}\text{Kr}$ , is used as marker. After oxidation thin, uniform layers of oxide, of known thickness, are removed and the activity remaining at each stage is measured, whereby the depth profile of the marker is easily established as shown in Figure 2.

The best and most extensive studies of this type have been made on the anodic oxidation of tantalum<sup>(1)</sup>. Anodic  $\text{Ta}_2\text{O}_5$  can be dissolved very uniformly by a solution of  $\text{HF}$  and  $\text{NH}_4\text{F}$ . Furthermore the oxide shows good interference colours and by

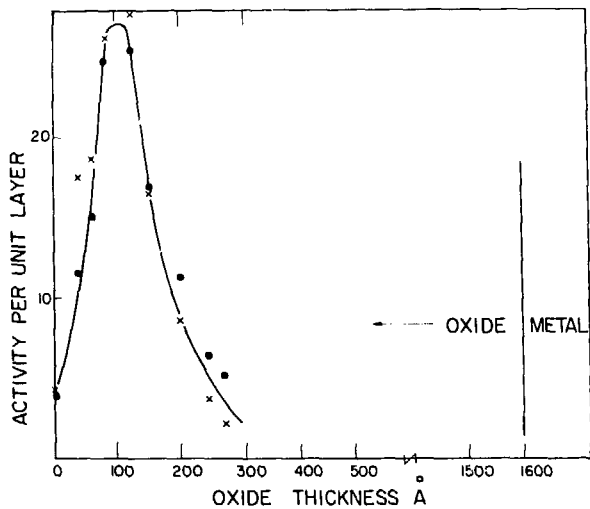


Figure 2 Depth profile of  $^{125}\text{Xe}$  in zirconium after anodic oxidation.

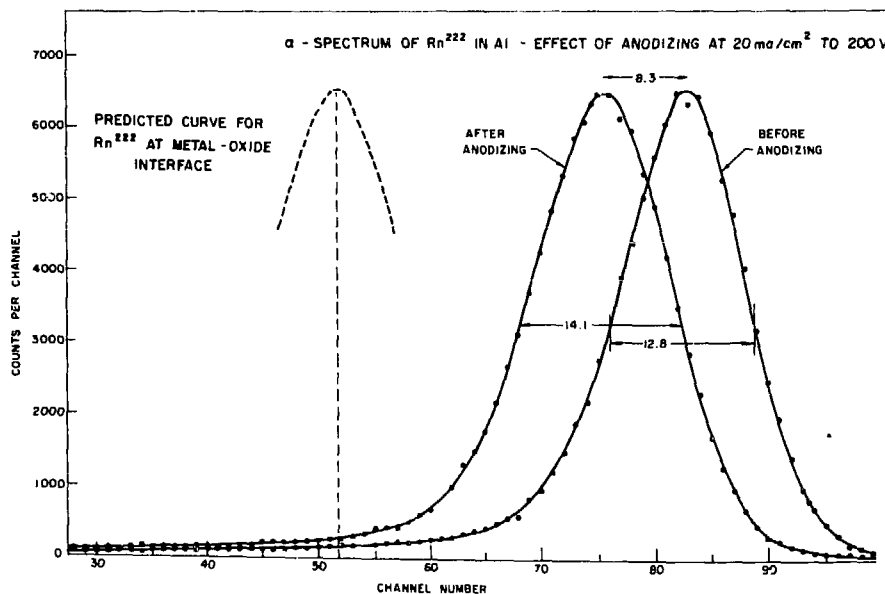
using a spectrophotometer the initial thickness of oxide and the thickness remaining after each stripping cycle can be measured accurately.

Uniform chemical stripping is not possible with many oxides, hence in studying anodic oxidation of zirconium<sup>(2)</sup> it was necessary to remove layers of oxide by a vibratory polishing machine. Anodic  $\text{ZrO}_2$  also shows good interference colours hence the thickness measurements could again be made with the spectrophotometer.

The second class of experiments relies on the fact that energetic charged particles, such as electrons or helium ions, lose energy as they pass through solids. The simplest example is probably the work on anodic oxidation of aluminum and tantalum<sup>(3)</sup> using, as marker, the radio-tracer  $^{222}\text{Rn}$  which is an  $\alpha$ -emitter. The energy of the emitted helium ions after implanting the  $^{222}\text{Rn}$ , but before anodizing, was measured using a solid-state detector and a pulse height analyser. After anodizing, the helium ion energy was measured again and found to have decreased (Fig. 3). The decrease in energy can be related to the depth of the  $^{222}\text{Rn}$  using published data on stopping powers for helium ions, i.e. on the rate of energy loss per unit distance. The total thickness of oxide can be found from known voltage-thickness relationships.

A similar type of experiment was used to study anodic oxidation of aluminum, niobium, tantalum, tungsten, zirconium and hafnium<sup>(4)</sup>. In this case the marker was  $^{125}\text{Xe}$  which decays by emitting 21.8 keV conversion electrons whose energy was measured extremely accurately using the  $\pi\sqrt{2}$   $\beta$ -spectrometer.

Figure 3 The  $\alpha$ -spectrum of  $^{222}\text{Rn}$  in aluminum before and after anodic oxidation. The dotted line is the spectrum that would have resulted if the  $^{222}\text{Rn}$  had been located at the metal-oxide interface. One channel is equivalent to 1.74 keV.



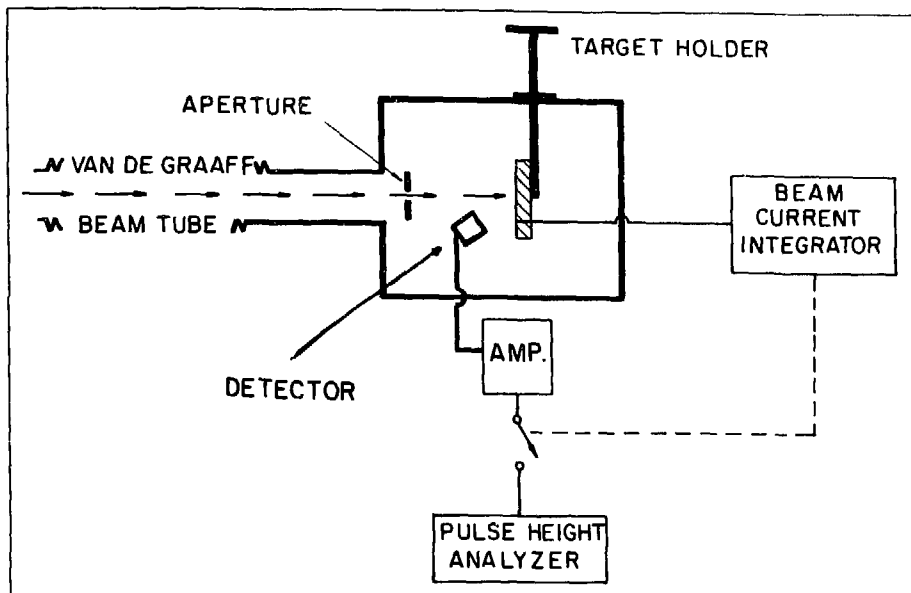


Figure 4 Schematic diagram of the equipment used to record the spectra of backscattered He ions.

Figure 5 Spectrum of the ions backscattered from an aluminum target implanted with Xe. The sharp peak arises from ions scattered by Xe and the continuum from ions scattered by the aluminum.

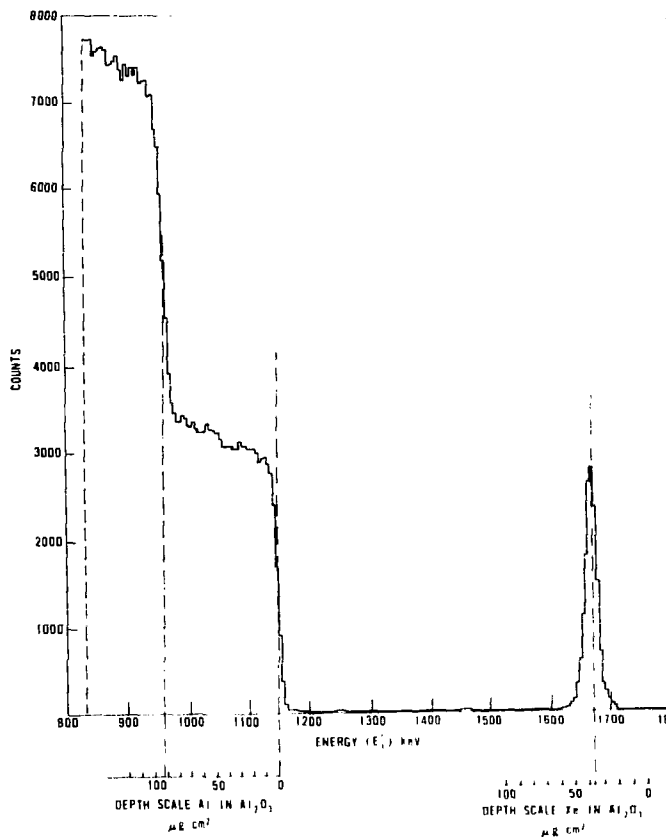
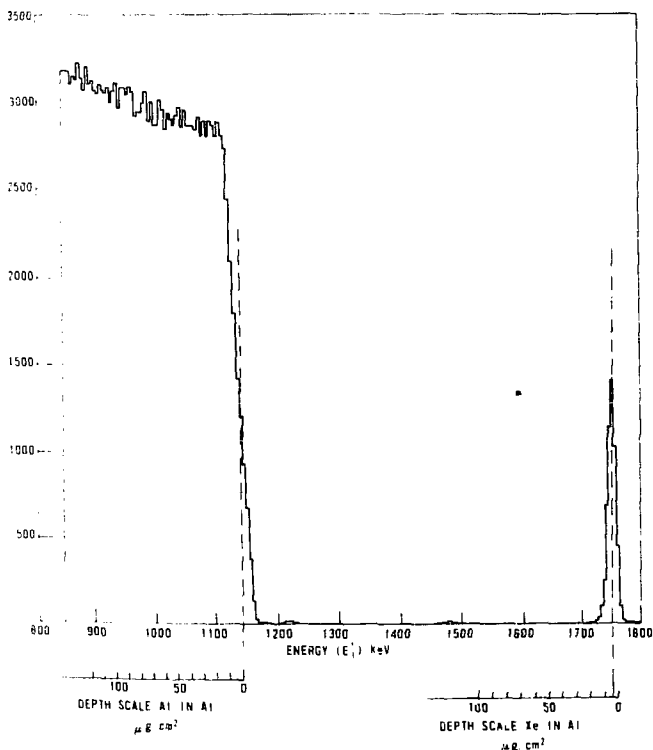


Figure 6 The same as Fig. 5 except that the specimen has been anodized. The Xe peak has shifted to lower energy and the continuum contains a step whose width gives the thickness of the oxide.

Again, the energy shift that occurs when the specimen is anodized can be related to the depth of the  $^{125}\text{Xe}$  and as before, the total oxide thickness must be obtained from a voltage-thickness calibration.

A more recent modification of the same basic idea is the use of Rutherford backscattering to study anodic oxidation of aluminum<sup>(5)</sup>. As in the case of the  $^{222}\text{Rn}$  experiments the technique relies on measuring energy spectra of helium ions. However, in this case the helium ions do not originate from radio-active decay of the marker atom. Instead, the aluminum specimen, implanted with stable xenon atoms, is bombarded with 2 MeV helium ions from a Van de Graaff accelerator and energy spectra of the ions scattered backwards are recorded (Fig. 4). Spectra are obtained before and after anodizing. Some of the ions have been scattered from the marker atoms (Xe) and from a knowledge of the kinematics of the scattering process and the stopping powers, the depth of the xenon atoms can be established. Other ions are scattered by the aluminum atoms and since the concentration of aluminum atoms in the oxide is lower than in the metal the number of backscattered ions, as a function of their energy, can be analyzed to give the thickness of the oxide. Thus the spectra contain the required information on both the marker position and the oxide thickness; this point is illustrated in Figures 5 and 6.

In total, the experiments at CRNL have covered anodic oxidation of aluminum, niobium, tantalum, tungsten, zirconium and hafnium. For the first four metals the results show that both metal and oxygen are mobile during anodizing whereas for the last two only the oxygen is mobile. Preliminary results indicate that silicon probably falls into this second category. In the case of tantalum the effects of changing temperature and current density have been investigated in some detail<sup>(1)</sup> and found to make small (less than 10%) but detectable, changes to the transport numbers. The apparent transport number of aluminum anodized in ammonium citrate has also been shown to vary with current density<sup>(4)</sup>. This effect is partly caused by the fact that at low current density some aluminum dissolves in the electrolyte, thus lowering the measured aluminum transport number. It has also been associated with the fact that at very low current density the oxides are porous and hence the whole transport mechanism can be quite different from that operating in a true barrier oxide.

Although this review has dealt, so far, with the use of inert markers in anodic oxidation, the associated techniques are applicable to many other situations. Vibratory polishing has been used to study the

behaviour of ion-implanted rubidium and bromine during the anodic oxidation of zirconium and also the behaviour of bromine incorporated into anodic zirconium oxide from the electrolyte<sup>(2)</sup>. The behaviour of the bromine is strikingly different under these two conditions. Implanted bromine is truly 'trapped' in the oxide and remains at the outer surface. Bromine from the electrolyte penetrates through the oxide, indicating some degree of porosity. Chemical stripping has been used in preliminary experiments to study the fate of sulphate ions when tantalum is anodized in an electrolyte containing  $^{35}\text{SO}_4$  ions. Rutherford scattering is currently being used to study the behaviour of a wide variety of implanted foreign atoms during anodic oxidation of aluminum; there are remarkable differences between the behaviour of foreign atoms according to whether they are implanted into the metal or into a thin oxide layer pre-formed on the metal. There have been preliminary investigations into the behaviour of alloying elements during anodic oxidation of aluminum. In view of the current interest in ion implantation as a means of producing semi-conductor devices we are studying the behaviour of implanted atoms during anodic oxidation of silicon. Also, since silicon is extremely susceptible to radiation damage we are attempting to see whether damage plays any role in the oxidation process.

F. Brown

## REFERENCES

1. J.P.S. Pringle, Extended Abstracts of the 135th National Meeting of the Electrochemical Society, May 4-9, 1969, page 17.
2. J.L. Whitton J. Electrochemical Soc. 115 (1968) 58.
3. J.A. Davies and B. Domeij, J. Electrochemical Soc. 110 (1963) 849
4. J.A. Davies, B. Domeij, J.P.S. Pringle and F. Brown. J. Electrochemical Soc. 112 (1965) 675.
5. W.D. Mackintosh Proceedings of the C.N.R.S. Colloquium on Activation Analysis, Saclay, October, 1972. To be published in J. Radio-analytical Chem.

\*

Additional copies of this document  
may be obtained from  
Scientific Document Distribution Office  
Atomic Energy of Canada Limited  
Chalk River, Ontario, Canada  
K0J 1J0

Price - \$1.00 per copy

3077-72